

Constraints on Dark Matter Annihilation/Decay from the Isotropic Gamma-Ray Background

Wei Liu, Xiao-Jun Bi, Su-Jie Lin, Peng-Fei Yin

Key Laboratory of Particle Astrophysics, Institute of High Energy Physics, Chinese Academy of Sciences, Beijing 100049, China

Abstract

In this work we study the constraints on dark matter (DM) annihilation/decay from the Fermi-LAT Isotropic Gamma-Ray Background (IGRB) observation. We consider the contributions from both extragalactic and galactic DM components. For DM annihilation, the evolutions of extragalactic DM halos are taken into account. We find that the IGRB constraints under some DM subhalo models can be comparable to those derived from the observations of dwarf spheroidal galaxies. We also use the IGRB results to constrain the parameter regions accounting for the latest AMS-02 electron-positron anomaly. We find that the majority of DM annihilation/decay channels are strongly disfavored by the latest Fermi-LAT IGRB observation; only DM annihilation/decay to $\mu^+\mu^-$ may be valid.

Keywords: dark matter theory, gamma-ray theory, dark matter simulations, gamma-rays: diffuse background

1. Introduction

From the numerous observations of the astrophysics and the cosmology, it is well confirmed that the dark matter (DM) constitutes about 84% of the total matter in the universe [1]. Despite of its proverbial existence, we still have a poor understanding on its microscopic properties. In many new physics models, a kind of weakly interacting massive particles(WIMPs) are well-motivated DM candidates. They are expected to either self-annihilate or decay into Standard Model particles, such as neutrinos, antiprotons, electrons/positrons, photons and so on. One kind of methods for the DM identification, namely DM indirect detection, is to search such signals from DM

annihilation or decay. Of particular interest is the gamma-ray observation with high sensitivity. Since the propagation process is simple and the energy loss is small, the photons are very powerful probes to reveal the DM property.

Recently, the Fermi-LAT collaboration reported their 4-year measurement of the diffuse isotropic gamma-ray background (IGRB) at high latitudes with $|b| > 10^\circ$ [2]. Compared with the previous measurements [3, 4], the new Fermi-LAT data further extend to higher energy range, from 0.1 GeV to 820 GeV, nearly four decades. Especially above 300 GeV, a significant high energy cut-off has been discovered. The whole spectrum can be well described by a single power-law plus an exponential cutoff with the index $\gamma \sim 2.32 \pm 0.02$ and $E_{\text{cut}} \sim 279 \pm 52$ GeV. The dominant component of the IGRB is believed to be originated from the extragalactic astrophysical sources, most of which are too faint or too diffuse to be resolved, such as blazars, mis-aligned active galactic nuclei and star-forming galaxies and so on. Some galactic sources, such as millisecond pulsars, can also contribute to the IGRB [5]. However, since the predicted intensity from astrophysical sources is highly model dependent, there still exists a possible contribution from DM annihilation or decay in the IGRB. Thus the IGRB is often considered to be a powerful probe to search for the DM signals, and has been used to set upper limits on the DM annihilation cross section or decay lifetime in several studies [6, 7, 8, 9, 10, 11, 12, 13, 14, 15, 16, 17, 18, 19, 20, 21, 22, 23, 24].

On the other hand, a hot issue has received considerable attention in the DM study. In recent years, several experiments, such as PAMELA [25], ATIC [26] and Fermi [27], reported an excess of the cosmic ray electron-positron measurement. Most recently, the AMS-02 results [28, 29] have confirmed such excess from $\sim 0.5 - 500$ GeV with a high precision. This anomaly can be explained by the DM with a large annihilation cross section to charged leptons, which is several orders of magnitudes over the thermal freeze-out value $3 \times 10^{-26} \text{ cm}^{-3} \text{ s}^{-1}$. Such DM particles would also inevitably induce significant gamma-ray signals by the cascade decay, internal bremsstrahlung, final state radiation (FSR), and the inverse Compton scattering (ICS) of electrons to background radiation field. Therefore, the IGRB is naturally summoned up as a powerful tool to constrain the DM explanations of the positron excess.

In this work, we study the constraints on the DM annihilation cross section and decay lifetime by using the latest Fermi-LAT IGRB results, and compare these limits with the DM parameter space which can explain the latest AMS-02 electron-positron observation. Compared with the previous

works, we have made following improvements:

1. Both extragalactic and galactic contributions of DM annihilation/decay are reckoned. The steady-state spatial distribution of electrons and corresponding ICS gamma-rays in the Galaxy are computed by GALPROP ¹ [30, 31] with the comprehensive consideration of the transport equation and the background radiation field.
2. Three kinds of limits, namely conservative, background-fixed, and background-relaxed, are adopted and compared with each other. The goodness of bound depends on the limit method. Especially we show that the shape of bound curves could vary with constraint methods.
3. New cosmic-ray data have been extensively applied. We consider recent AMS-02 proton [32], B/C [33] and electron-positron data [28, 29]. They are used to constrain transport parameters in the Galaxy [34, 35], and obtain the updated DM parameter space favored by cosmic-ray positron anomaly.

The paper is organized as follows: In section II, we give a comprehensive introduction to the gamma-ray flux from DM annihilation(or decay). For the extragalactic DM annihilation, the dominant theoretical uncertainties arise from the unclear clustering history and properties of small DM halos. We consider these uncertainties under different assumptions about minimum DM halos. In section III, we discuss the limit approach to the DM annihilation(or decay). Then we illustrate our analysis of results. We derive the constraints under some different concentration models in DM annihilation. But for the decaying DM, due to that there are no above uncertainties, the constraints are quite confirmative. We also use GALPROP to calculate the propagation of the DM induced electrons and positrons, and obtain the parameter space accommodating the AMS-02 results. We compare these parameter space with the IGRB constraints. Finally, the summary are given in Section IV.

2. Diffuse Gamma-Rays from Dark Matter Annihilation/Decay

Both the extragalactic and galactic DM can produce high energy photons. The gamma-ray flux induced by extragalactic DM depends on the history of

¹<http://galprop.stanford.edu>

DM clustering and is essentially isotropic. On the other hand, the spatial distribution of the galactic gamma-ray signal is apparently anisotropic due to our special position in the Galaxy. Even after rigorously subtracting anisotropic component of galactic gamma-rays, there would still exist an residual isotropic component in the IGRB, which is equal to the signal from the direction of anti galactic center. Thus both the extragalactic and galactic DM would contribute to the IGRB signal, and the expected DM-induced IGRB flux can be written as [12, 15, 16]

$$\Phi^{\text{DM}} = \Phi_{\text{EG}}^{\text{DM}} + \Phi_{\text{G}}^{\text{DM}} \Big|_{\text{antiG}}. \quad (1)$$

2.1. Gamma-Rays from Cosmological Dark Matter Evolution

The total gamma-ray flux emitted from the extragalactic annihilating DM at different redshifts is given by [6, 11, 16],

$$\Phi_{\text{EG}}^{\text{anni}}(E, z) = \frac{c(1+z)^2 \Omega_{\chi}^2 \rho_c^2 \langle \sigma v \rangle}{4\pi 2m_{\chi}^2} \int_z^{\infty} dz' \frac{(1+z')^3 [\Delta^2(z') + 1]}{H(z')} \frac{dN}{dE'} \exp[-\tau(z; z', E')], \quad (2)$$

where m_{χ} is the mass of DM particle, and $\langle \sigma v \rangle$ is the corresponding thermal averaged annihilation cross section. $H(z) = H_0 \sqrt{(\Omega_{\chi} + \Omega_b)(1+z)^3 + \Omega_{\Lambda}}$ and $\rho_c = 3H_0^2/8\pi G$ are the Hubble parameter at redshift z and current critical density of the Universe, respectively. For the latest cosmological parameters Ω_{χ} , Ω_b , Ω_{Λ} and h , we refer to the values from [36]. $\Delta^2(z)$ denotes the enhancement of DM annihilation, and will be introduced in a great detail in the next subsection. In eq. (2), z and z' are redshifts at which photons are observed and emitted respectively. dN/dE' indicates the initial gamma-ray spectrum per DM pair annihilation, and $E' \equiv E(1+z')/(1+z)$ is the photon energy at redshift of emission z' . The prompt photons from DM annihilation are produced by the final-state radiations or cascade decays of the annihilation products. In this work, the injected energy spectrum of prompt photons is generated by PPPC4DMID[37].

The photons can also come from the ICS by DM-induced electrons and positrons off the interstellar radiation field, such as the cosmic microwave background(CMB), infrared photons and starlight. The gamma-ray flux from the ICS process is given by

$$\frac{dN}{dE} \Big|_{\text{IC}} = c \int d\epsilon n(\epsilon) \int dE_e \frac{dn}{dE_e} \times F_{\text{KN}}(\epsilon, E_e, E), \quad (3)$$

where $n(\epsilon)$ is the number density distribution of the background radiation as a function of energy ϵ at redshift z . For the cosmological ICS process, we only take into account the CMB photons. dn/dE_e is the energy spectrum of electrons. In this work, we adopt the assumption that electrons quickly lose their energy and the resulting distribution of electrons reaches equilibrium [8, 11]. Hence the spectrum is evaluated by equating the injected rate of DM electrons with the corresponding energy loss rate, which can be written as

$$\frac{dn}{dE_e} = \frac{1}{b(E_e, z)} \int_{E_e}^{m_\chi} dE'_e \frac{dN_e}{dE'_e}. \quad (4)$$

with the energy loss rate $b(E_e, z) \approx 2.67 \times 10^{-17} (1+z)^4 (E_e/\text{GeV})^2 \text{ GeV s}^{-1}$. The differential Klein-Nishina cross section $F_{\text{KN}}(\epsilon, E_e, E)$ is adopted as the following form [38, 39]

$$F_{\text{KN}}(\epsilon, E_e, E) = \frac{3\sigma_T}{4\gamma^2\epsilon} \left[2q \ln q + (1+2q)(1-q) + \frac{(\Gamma q)^2(1-q)}{2(1+\Gamma q)} \right], \quad (5)$$

where σ_T is the Thomson cross section, γ is the Lorentz factor of electron, $\Gamma = 4\epsilon\gamma/m_e$, and $q = E/\Gamma(E_e - E)$. On a separate note, when $q < 1/4\gamma^2$ or $q > 1$, $F_{\text{KN}}(\epsilon, E_e, E) = 0$.

2.2. Clumpiness Factor of Dark Matter Annihilation

As the DM annihilation rate is proportional to the square of number density, ρ^2 , the annihilation signal would be significantly enhanced in the clumpy halos. The enhancement factor $\Delta^2(z)$ can be defined as summing up the contributions of all the halos with different masses formed in the history of Universe

$$\Delta^2(z) = \frac{\Delta_{\text{vir}}(z)}{3\rho_\chi} \int dM_{\text{vir}} M_{\text{vir}} \frac{dn(z)}{dM_{\text{vir}}} \frac{\int \tilde{\rho}^2(x) x^2 dx}{\left(\int \tilde{\rho}(x) x^2 dx\right)^2} x_{\text{max}}^3, \quad (6)$$

where M_{vir} is the virial mass of the DM halo, $dn(z)/dM_{\text{vir}}$ is the halo mass function, and $\tilde{\rho}$ is defined to describe the inner density profile of a single DM halo. Due to the self-similarity in the halo formation, all the halos share a common profile. Here we adopt the well-known NFW profile [40]

$$\tilde{\rho}(x) = \frac{\rho}{\rho_s} = \frac{1}{x(1+x)^2} \quad (7)$$

with $x \equiv r/r_s$. The scale radius r_s is related to the virial radius r_{vir} through

$$r_s = \frac{r_{\text{vir}}}{c_{\text{vir}}}. \quad (8)$$

The virial radius r_{vir} can be directly derived from the virial mass M_{vir}

$$r_{\text{vir}} = \left(\frac{3M_{\text{vir}}}{4\pi\Delta_{\text{vir}}(z)\rho_{\chi}(z)} \right)^{1/3}, \quad (9)$$

where $\rho_{\chi}(z) = \rho_{\chi}(1+z)^3$ is the mean DM density at redshift z . The virial overdensity $\Delta_{\text{vir}}(z)$ is taken to be [41]

$$\Delta_{\text{vir}}(z) = (18\pi^2 + 82y - 39y^2)/(1+y), \quad (10)$$

with $y = \Omega_m(z) - 1$ and $\Omega_m(z) = \Omega_m(1+z)^3/(\Omega_m(1+z)^3 + \Omega_{\Lambda})$.

In eq. (8), the concentration parameter c_{vir} is a function of the virial mass M_{vir} and redshift z . The value of c_{vir} is usually obtained from the N-body simulation. However, the halos with low masses are beyond the power of the state-of-the-art resolution. Thus their c_{vir} is roughly evaluated by the extrapolation according to the fitting formula within the reach of simulations. The DM-induced gamma-ray flux can be enhanced by the promoted concentration as a result of the larger annihilation rate. In the cold dark matter(CDM) scenario, the structures are organized by 'bottom-up' fashion, i.e. the smaller structures formed earlier than larger ones. Since those massive halos assemble later and experience recent major merger, they typically hold lower concentrations compared with those growing quiescently and with smaller mass. This means that the concentration varies inversely with the halo mass [42]. Thus the gamma-ray intensity is sensitive to the lower halo mass cut-off and the slope of the concentration model. Here we consider two concentration models: one is an analytical model developed in [43] (B01), and the other is a direct extrapolation of the fitting results from the simulation [44](M08). In the above models, we assume the linear redshift evolution of the concentration parameter, i.e. $c_{\text{vir}}(z) = c_{\text{vir}}(z=0)/(1+z)$ [43].

In this section, we compute the diffuse gamma-ray contributions of four DM benchmark points listed in Table. 1. These parameter points are derived from a Markov Chain Monte Carlo (MCMC) fitting [45] to the latest AMS-02 electron/positron measurements [28, 29]. In the left panel of Figure 1, we show the extragalactic DM-induced gamma-ray spectra under two different concentration models. The dashed and dash-dot lines represent the spectra

in the models of B01 and M08, respectively. Here the minimum DM halo mass is taken to be $M_{\min} = 10^{-6} M_{\odot}$. Although both B01 and M08 models provide a good fitting to the concentration parameters within the resolution of the N-body simulation, the different extrapolations in the low halo mass region still produce nearly one order of magnitude difference. On the other hand, the low mass cutoff of the DM halo is also unclear due to the limited resolution of the N-body simulation. In the right panel of Figure 1, we show the gamma-ray spectra for different assumptions of the minimum DM halo mass $M_{\min} = 10^{-9}$, 10^{-6} , and $10^5 M_{\odot}$ in the B01 model. We can see that the gamma-ray intensity gradually raises with M_{\min} decreasing. In the rest of this paper, we always take the minimum halo mass to be $M_{\min} = 10^{-6} M_{\odot}$. Note that here the effect of extragalactic background light has been include, which will be expatiated in the next subsection.

Channel	Annihilation		Decay	
	m_{χ} (GeV)	$\langle\sigma v\rangle$ ($10^{-23} \text{ cm}^3\text{s}^{-1}$)	m_{χ} (GeV)	τ (10^{26} s)
$\mu^+\mu^-$	417.44	0.30	808.63	9.13
$\tau^+\tau^-$	1007.84	2.11	1774.76	3.21

Tab. 1: The best-fit values of mass-cross section(decay lifetime) parameter space for the latest AMS-02 positron-electron data [28, 29]. The DM are chosen to annihilate(decay) into $\mu^+\mu^-$ and $\tau^+\tau^-$ channels.

2.3. Extragalactic background light

The factor $\exp[-\tau(z; z', E')]$ characterizes the absorption of gamma-ray photons when crossing the universe. $\tau(z; z', E')$ is the optical depth of gamma photons between observed redshift z and emission redshift z' , and is obtained by following relation:

$$\tau(z; z', E') = c \int_z^{z'} dz'' \frac{\alpha(E'', z'')}{H(z'')(1+z'')}, \quad (11)$$

where $E'' = E'(1+z'')/(1+z')$, and $\alpha(E, z)$ is the absorption coefficient. As far as we are concerned, the dominant energy loss of high energy photons is the scattering with extragalactic UV background light. In this work, we refer to the UV background model given by [46]. The UV background mainly affects the gamma-ray flux above 100 GeV, which is suppressed by roughly

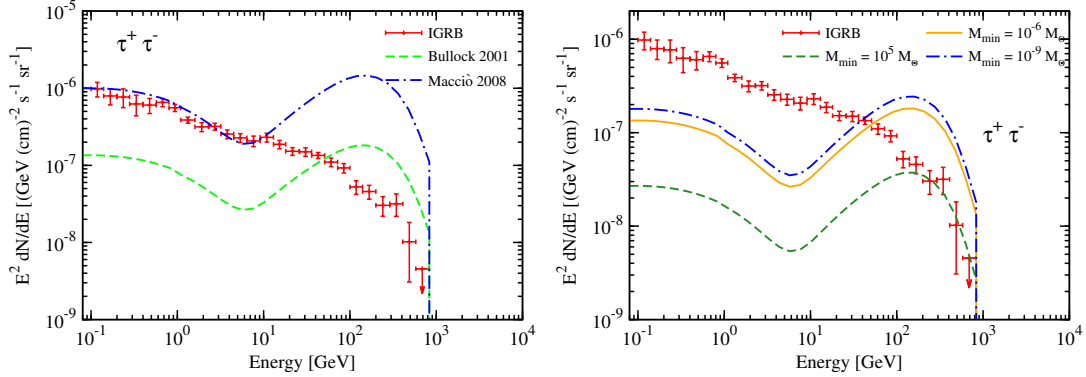


Fig. 1: Left: the extragalactic gamma-ray spectra due to different sets of the concentration parameter c_{vir} . The annihilation channel is chosen to be $\chi\chi \rightarrow \tau^+\tau^-$. The green dashed and blue dash-dot lines represent the spectra in the models of B01 [43] and M08 [44], respectively. Here the minimum DM halo mass is $M_{\text{min}} = 10^{-6} M_{\odot}$. Right: the same gamma-ray spectra assuming different minimum DM halo masses. The blue dash-dot, yellow solid and green dash lines correspond to $M_{\text{min}} = 10^{-9}, 10^{-6}, 10^5 M_{\odot}$ in the B01 model.

one order of magnitude. Besides we still consider other energy loss processes: pair production on neutral matter ($6 < z < 1000$), pair production on fully ionized matter ($z < 6$), photon-photon scattering and photon-photon pair production with the CMB photons [37]. These interactions give a very small contribution to the attenuation of high energy gamma-ray photons.

In the left panel of Figure 2, we show the extragalactic gamma-ray spectra with and without the absorption effect of extragalactic background light. The annihilation is chosen to be $\chi\chi \rightarrow \tau^+\tau^-$ channel. Here the concentration model is chosen to be B01. It is apparent that EBL mainly influence the high energy gamma-ray spectra, above tens of GeV. The blue dash and purple solid lines are the galactic gamma-ray flux and total flux with EBL.

2.4. Diffuse Gamma-Rays from Galactic Dark Matter annihilation

The gamma-ray signal from the annihilation of Galactic DM particles is obtained by the light-of-sight integral of squared DM density at an angle ψ with respect to the direction of galactic center. The prompt radiation is given by

$$\Phi_{\text{G}}^{\text{Prompt}}(E, \psi) = \langle \sigma v \rangle \frac{R_{\odot} \rho_{\odot}^2}{8\pi m_{\chi}^2} \frac{dN}{dE} \int_{l.o.s.} \left[\frac{\rho(r(x, \psi = \psi(b, \ell)))}{\rho_{\odot}} \right]^2 \frac{dx}{R_{\odot}}. \quad (12)$$

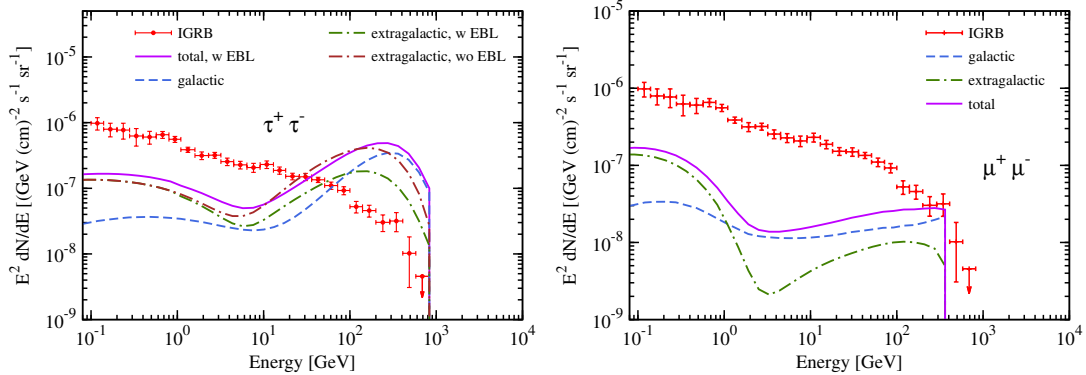


Fig. 2: Left: the influence of extragalactic background light (EBL). The green dash-dot and brown dash-dot lines represent the extragalactic flux with and without EBL. The blue dash line is the galactic contribution. The purple solid line is the total flux with EBL. The annihilation channel is $\chi\chi \rightarrow \tau^+\tau^-$. Right: the galactic (blue dash line), extragalactic (green dash-dot line) and total (purple solid line) gamma-ray flux from $\chi\chi \rightarrow \mu^+\mu^-$ channels of DM annihilation. Both DM particle's cross section and mass are listed in the table 1.

$r(b, \ell, x) = \sqrt{R_\odot^2 - 2xR_\odot \cos(\ell) \cos(b) + x^2}$ is the distance to the galactic center, where (b, ℓ) are the galactic coordinates. Due to the finite resolution of the telescope, the gamma-rays actually are received from a finite observational solid angle. Therefore the predicated gamma-ray flux from DM annihilation should be averaged within a solid angle $\Delta\Omega$ toward an observational region

$$\bar{\Phi}_G^{\text{Prompt}}(E, \psi) = \langle \sigma v \rangle \frac{R_\odot \rho_\odot^2}{8\pi m_\chi^2} \frac{dN}{dE} \int_{\Delta\Omega} \frac{d\Omega}{\Delta\Omega} \int_{l.o.s.} \left[\frac{\rho(r(b, \ell, x))}{\rho_\odot} \right]^2 \frac{dx}{R_\odot}. \quad (13)$$

We find that for the case of anti-galactic direction, this average brings about negligible improvement. For the density distribution of the Galactic DM halo, we still adopt the NFW density profile with fixing the local DM density $\rho(r = r_\odot) = 0.3 \text{ GeV/cm}^3$ and total DM mass within 60 kpc $M(\leq 60 \text{ kpc}) = 4.7 \times 10^{11} M_\odot$, which means $r_s = 24.42 \text{ kpc}$ and $\rho_s = 0.184 \text{ GeV/cm}^3$ [37].

For the gamma-rays from the ICS by DM-induced high energy electrons, we need to solve the transport equation of electrons in the Galaxy. However, the high energy electrons can only transport a few hundreds of parsecs due to the significant energy loss. Thus the observed electrons are mainly originated from the nearby sources. Unlike the extragalactic ICS process, the background photons include two additional components as well as the CMB

photons: infra-red light from the absorption and re-emission of starlight by galactic dust and starlight from stars in the galactic disk. Both of them mostly distribute in the Galactic disk and are spatial dependent. Yet the usual analytical solutions of transport equation often make simplified assumption on the radiation field. In this work, the package GALPROP is used to numerically solve the transport and ICS processes of electrons, in which the spatial distribution of background radiations has been included. The spectra of initial electrons injected by DM are still evaluated by PPPC4DMID [37]. The transport parameters are consistent with those used to explain the latest AMS-02 results [34].

For the galactic DM annihilation, we still consider the boost factor due to DM substructures. Many analytic arguments and numerical simulations have confirmed the presence of substructure in the galactic DM halo [49, 50, 51]. We refer to the analytic substructure model developed by [52, 53]. This method can extend to the mass scales which are too small to be resolved by the numerical simulations.

In Figure 2, we compare the galactic gamma-ray flux with the extragalactic contribution. The annihilation channels are respectively $\chi\chi \rightarrow \tau^+\tau^-$ and $\chi\chi \rightarrow \mu^+\mu^-$. For $\tau^+\tau^-$ channel, the prompt radiation makes the stronger contribution. The galactic contribution exceeds the extragalactic one at higher energy, about hundreds of GeV. But for $\mu^+\mu^-$ channel, the prompt radiation flux is significantly weaker than ICS flux, thus the galactic flux holds a dominant position from lower energy, about several GeVs.

2.5. Gamma-rays from DM decay

Compared with the annihilating DM, the gamma-ray intensity from the decaying DM is only proportional to the cosmological DM density ρ_χ . Thus it does not suffer from enormous uncertainties, such as density profile of DM halo, the history of structure formation, concentration parameter, halo mass function and so on. In this case, the resulting predictions would be relatively more solid. The accumulated DM-induced gamma-ray flux during the evolution of universe is given by [12, 13, 15]

$$\Phi_{\text{EG}}^{\text{dec}} = \frac{c}{4\pi} \frac{\Omega_\chi \rho_c}{m_\chi \tau_{\text{dec}}} \int \frac{dz'}{H(z')} \frac{dN}{dE'} \exp[-\tau(z; z', E')], \quad (14)$$

with τ_{dec} the decay lifetime of DM particle. For the prompt contribution from galactic DM decay, we just need to make following substitution in eq.

(13):

$$\frac{\rho^2 \langle \sigma v \rangle}{2m_\chi^2} \rightarrow \frac{\rho}{m_\chi \tau} . \quad (15)$$

The spatial distribution and energy spectrum of electrons from galactic DM decay, and the ICS contribution to photons are also evaluated by GALPROP.

The left and right panels of Figure 3 show the gamma-ray spectra for $\chi\chi \rightarrow \tau^+\tau^-$ and $\chi\chi \rightarrow \mu^+\mu^-$ channels, respectively. Both the galactic (short dash) and extragalactic(dash-dot) contributions are also shown.

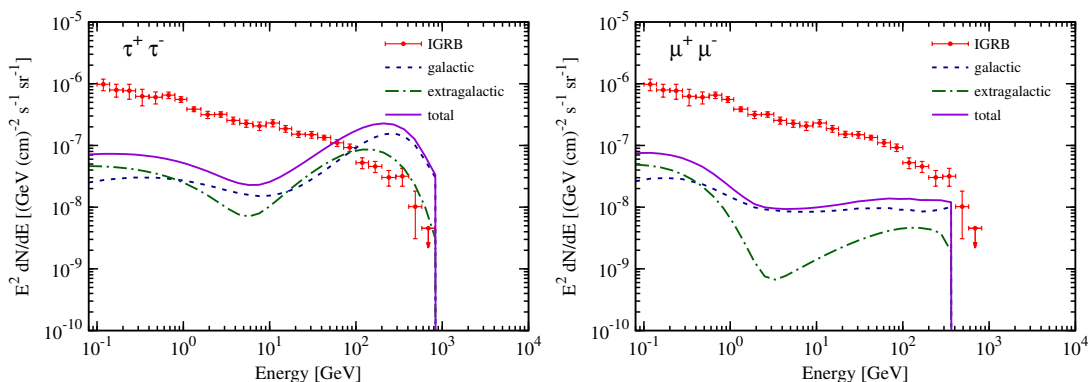


Fig. 3: The figure shows the galactic(blue dash line), extragalactic(green dash-dot line) and total(purple solid line) gamma-ray flux from different DM decay channels. The left is $\chi\chi \rightarrow \tau^+\tau^-$ channel, and the right is $\chi\chi \rightarrow \mu^+\mu^-$ channel. The cross section and mass are listed in the table 1.

3. Constraints on Dark Matter Annihilation/Decay

3.1. Methods

The main component of the observed IGRB is believed to be originated from unresolved astrophysical sources. In principle, the DM-induced signals can be obtained by subtracting all the astrophysical contributions from the Fermi-LAT data. The possible dominant candidates include blazars (including Flat Spectrum Radio Quasars and BL Lacertae) [54, 55, 56], star-forming galaxies [57, 58], misaligned AGN [59, 60]. Recent years, some authors have performed analysis by fitting the IGRB data with the astrophysical contributions along with their predicted theoretical uncertainties, and then set upper limits on the DM contribution[17, 18, 20, 21, 22]. Some studies claimed that the extragalactic gamma-ray background above 50 GeV can be principally

attributed to blazars [61]. However, the precise contributions of different populations are model dependent and remain unclear. In this work, we do not focus on the predictions and uncertainties of signatures from astrophysical sources, while adopting some model-independent methods to set constraints on DM annihilation/decay.

Conservative limits: As a first analysis, we require that the DM contributions alone should not exceed the observed IGRB spectra. The derived constraint is usually regarded as the most conservative one. The χ^2 can be defined in energy bins where the DM signal exceeds the IGRB intensity

$$\chi_{\text{cons}}^2 = \sum_{i \in \{i | \phi_i^{\text{DM}} > D_i^{\text{max}}\}} \frac{[D_i^{\text{max}} - \phi_i^{\text{DM}}]^2}{\sigma_i^2}. \quad (16)$$

ϕ_i^{DM} is the DM-induced gamma-ray flux in the i -th energy bin as a function of $\langle\sigma v\rangle$ or t_{dec} . We adopt the IGRB background based on the Galactic emission model A in Ref. [2]. We also incorporate foreground uncertainties into the IGRB spectra while with unchanged σ_i as Ref. [19]. All these new data points are called D_i^{max} . The corresponding 3σ DM limits are achieved when $\chi_{\text{cons}}^2 = 9$.

Background fixed: We assume a universal function to represent the total energy spectra from astrophysical sources. Its form is taken as a single power-law with an exponential cutoff at high energy

$$\phi^{\text{bg}} = I_0 \left(\frac{E}{100 \text{ MeV}} \right)^\gamma \exp \left(-\frac{E}{E_c} \right), \quad (17)$$

where I_0 , γ , and E_c are kept to be the best-fit values to the IGRB spectra under foreground model A [2]. The DM-induced photon flux is assumed to be superimposed on the background flux. This method is widely employed in the past studies [10, 15, 19]. The χ^2 is evaluated over all the energy bins:

$$\chi_{\text{sens}}^2 = \sum_i \frac{[D_i - \phi_i^{\text{bg}}(I_0, \gamma, E_c) - \phi_i^{\text{DM}}]^2}{\sigma_i^2}. \quad (18)$$

The 3σ limits are reached when the DM signal component forces the χ^2 to raise by more than 9 with respect to the best-fit χ^2 without DM signal.

Background relaxed: In this case, the astrophysical background is also assumed to be a single power-law plus an exponential cutoff, whereas I_0 , γ ,

and E_c are treated as free parameters as well as m_χ and $\langle\sigma v\rangle$ (or t_{dec}). For given m_χ and $\langle\sigma v\rangle$ (or t_{dec}), we can obtain a minimal χ^2 via a global fitting to the IGRB data. The upperlimit on $\langle\sigma v\rangle$ (or t_{dec}) can be obtained when corresponding χ^2 deviates from the minimal value χ_{min}^2 by a particular value. Here GNU Scientific Library(GSL)² is used to perform the nonlinear least-square fit.

3.2. Results

In this section, we show the IGRB limits on the DM annihilation cross sections for six different channels: e^+e^- , $\mu^+\mu^-$, $\tau^+\tau^-$, W^+W^- , $u\bar{u}$, and $b\bar{b}$ in Figure 4. Here we adopt the concentration model B01 [43] and set M_{min} to be $10^{-6} M_\odot$. Three types of the curves represent the constraints of conservative(blue), background-fixed(red) and background-relaxed(green) methods, respectively. We can see that, compared with the conservative limits, the background-fixed limits on the DM annihilation cross section can be improved by about one order of magnitude in the mass region of $\sim \mathcal{O}(10^2)$ GeV. The background-relaxed limits are always sandwiched between the conservative and background-fixed limits. For low DM masses, they are as stringent as the background-fixed limits. For the $\tau^+\tau^-$ and $u\bar{u}$ channels, these limits could even reach the thermal cross section $\langle\sigma v\rangle \sim 3 \times 10^{-26} \text{cm}^3\text{s}^{-1}$ at the mass region of $\sim \mathcal{O}(10)$ GeV. When the DM mass increases, all the constraints become loose and their distinctions decreases. As can be seen that the background-relaxed limits tend to the conservative limits at the DM mass region of $\mathcal{O}(10)$ TeV.

For comparison, the constraints from the latest Fermi-LAT observations of dwarf galaxies [62] are also shown in Figure 4. For the hadronic channels, the IGRB limits are always weaker than those of dwarf galaxies at low DM mass region. However, the IGRB observations could set stringent bounds for heavy DM particles annihilating to leptons as a result of large contributions from ICS processes. This is particularly clear for the e^+e^- channel as shown in Figure 4.

In Figure 4, we also show the parameter regions accounting for the cosmic-ray electron-positron anomaly renewed by the AMS-02 collaboration. The favored DM annihilation cross section and DM mass are derived from a global MCMC fit to the AMS02 data. We use the GALPORP to deal with the trans-

²<http://www.gnu.org/software/gsl/>

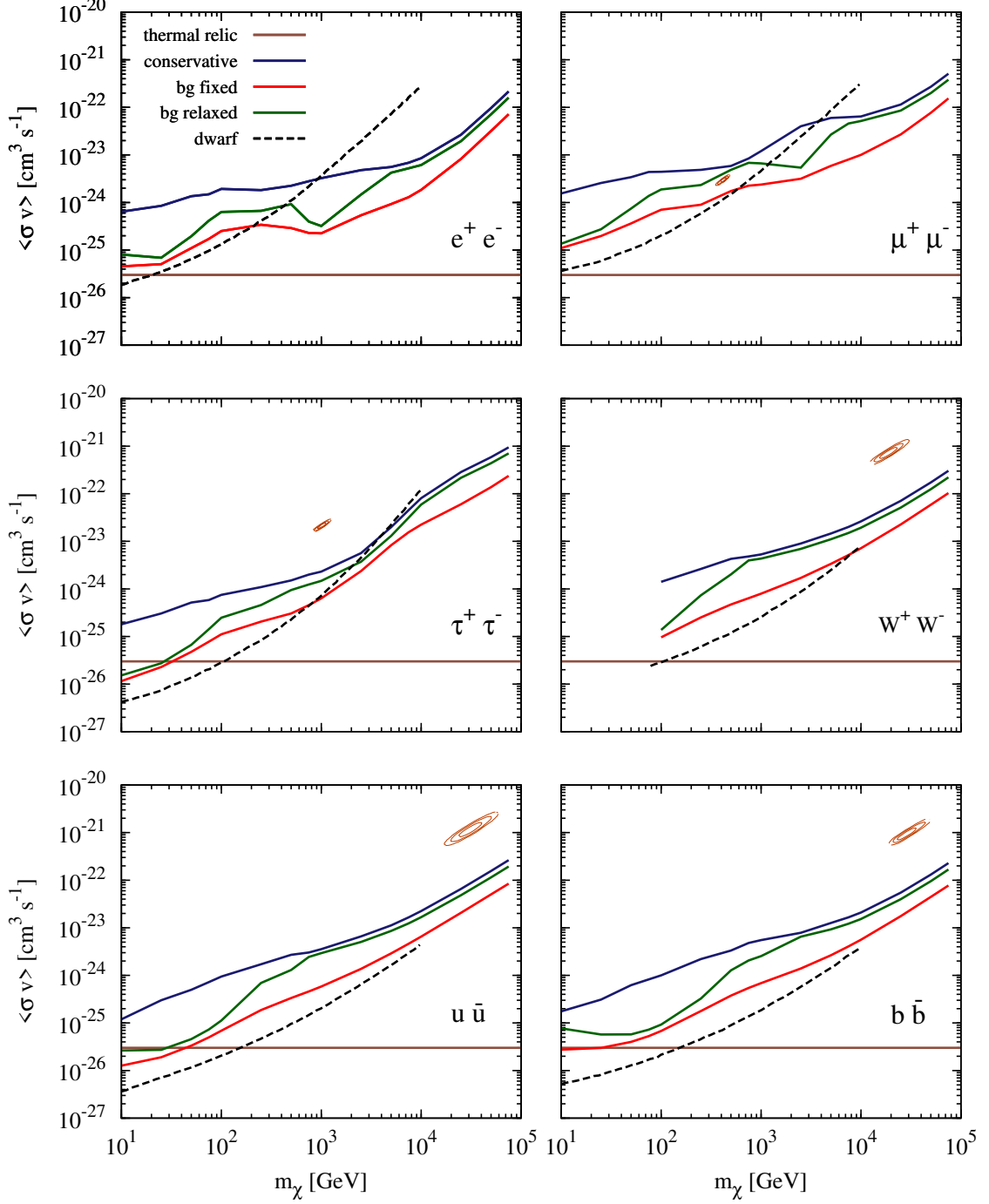


Fig. 4: The constraints on the DM annihilation cross section for six different DM annihilation channels: e^+e^- , $\mu^+\mu^-$, $\tau^+\tau^-$, W^+W^- , $u\bar{u}$, and $b\bar{b}$. The concentration model B01 [43] is adopted and $M_{\min} = 10^{-6} M_\odot$. The blue, red and green solid lines denote the conservative, background-fixed and background-relaxed limits, respectively. The brown solid line denotes the nature annihilation cross section for the thermal relic density $\sim 3 \times 10^{-26} \text{cm}^3 \text{s}^{-1}$. Black dash lines are the constraints from the Fermi-LAT observations of dwarf spheroidal galaxies [62]. The dark orange contours correspond to the 1 σ , 2 σ and 3 σ parameter regions accounting for the electron-positron excess observed by the AMS-02 [28, 29].

port effect, and adopt a conventional diffusion-convection model. More comprehensive discussions can be available in Ref. [34]. Here we do not consider the e^+e^- final states, since the corresponding sharp electron-positron spectra cannot fit the current AMS-02 data. As shown in figure 4, the available regions for $\mu^+\mu^-$ and $\tau^+\tau^-$ channels are much smaller than those for hadronic channels; DM masses required by the leptonic channels are also smaller than those for hadronic channels. We can see that almost all the channels have been excluded by the background-fixed IGRB limits. Only the parameter region for the $\mu^+\mu^-$ channel remains valid by the conservative IGRB limit.

In Figure 5 we show the IGRB limits on the DM annihilation cross section for the concentration model M08 [44]. All the limits are improved by almost one order of magnitude. This can be understood by the energy spectra shown in Figure 1. At low DM masses, the IGRB limits are already comparable to those from dwarf galaxies[62], which tend to $10^{27} \text{ cm}^3\text{s}^{-1}$. In this case, even the parameter space favored by the positron anomaly in $\mu^+\mu^-$ channel has been excluded readily by the conservative IGRB limit.

In Figure 6, we present the constraints on the lifetime of decaying DM. In contrast to DM annihilation, the gamma-ray fluxes generated by decaying DM are not significantly affected by the history of the structure formation. Therefore the constraints on the DM lifetime are more credible. The most stringent constraint comes from the e^+e^- channel, and reaches $\tau \sim 10^{28}\text{s}$ for the DM masses of $\mathcal{O}(1)$ TeV. This is because the main contributions of these two channels are photons from ICS and final state radiation processes, while the peak of energy spectra at high energies would become significant and easily constrained by Fermi-LAT data when DM mass increases. For the remaining channels, the limits are also stringent for low DM mass due to the contributions from cascade decay and hadronization processes. The regions in parameter space favored by the positron anomaly are also manifested. As can be seen that all the channels are disfavored by the background-fixed limits. Only the $\mu^+\mu^-$ channel remains allowed by the conservative limit.

4. Summary

In this work, we use the latest Fermi-LAT IGRB data to set upper limits on the DM annihilation cross section or the DM lifetime for six channels, i.e. e^+e^- , $\mu^+\mu^-$, $\tau^+\tau^-$, W^+W^- , $u\bar{u}$, and $b\bar{b}$. In order to consider the uncertainties from the multiplier of the extragalactic gamma-ray flux, the DM annihilation constraints are investigated in two competing parameterized concentration

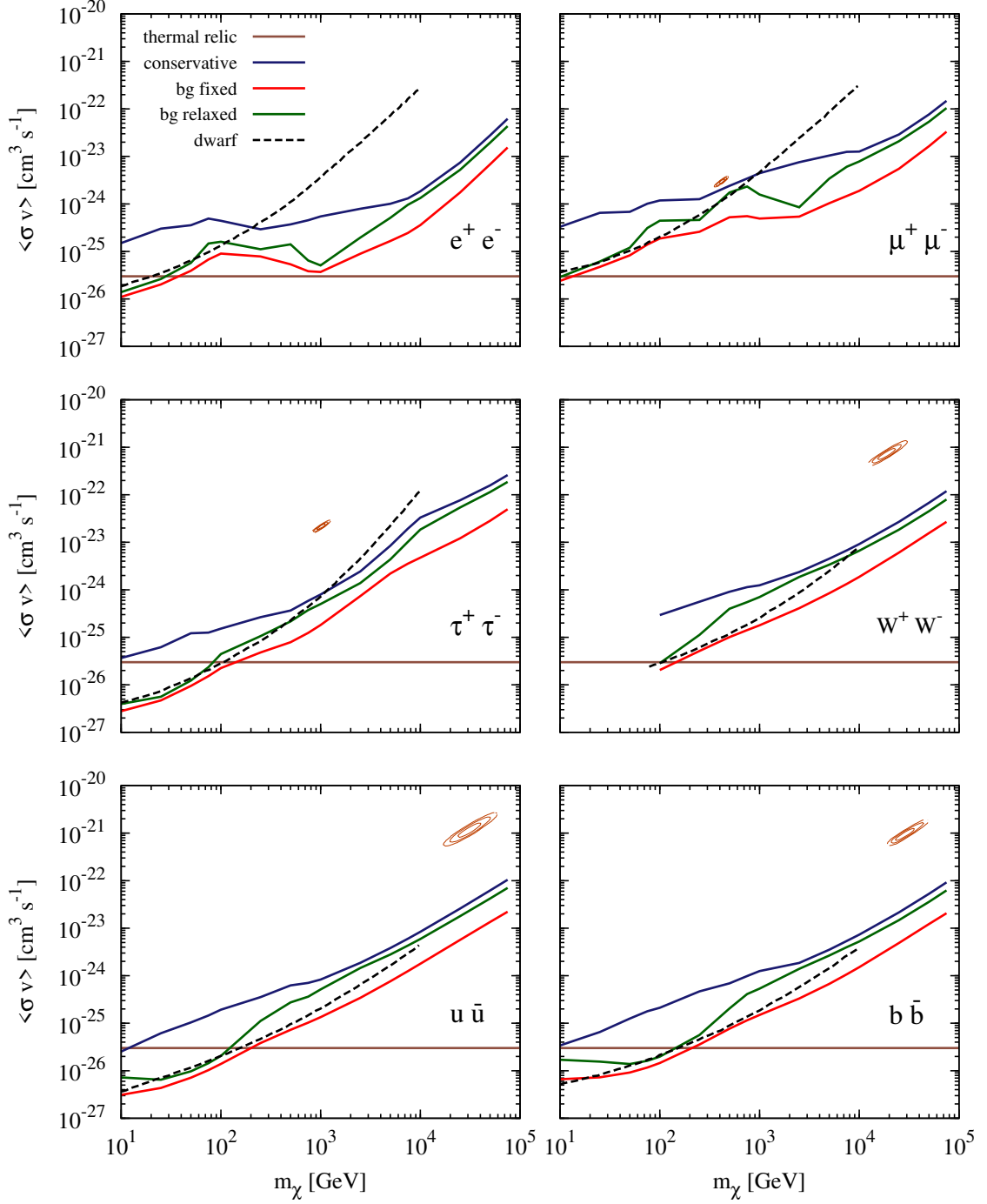


Fig. 5: The constraints on the DM annihilation cross section for six different DM annihilation channels. The concentration model M08 [44] is adopted. The notations are the same as Fig. 4.

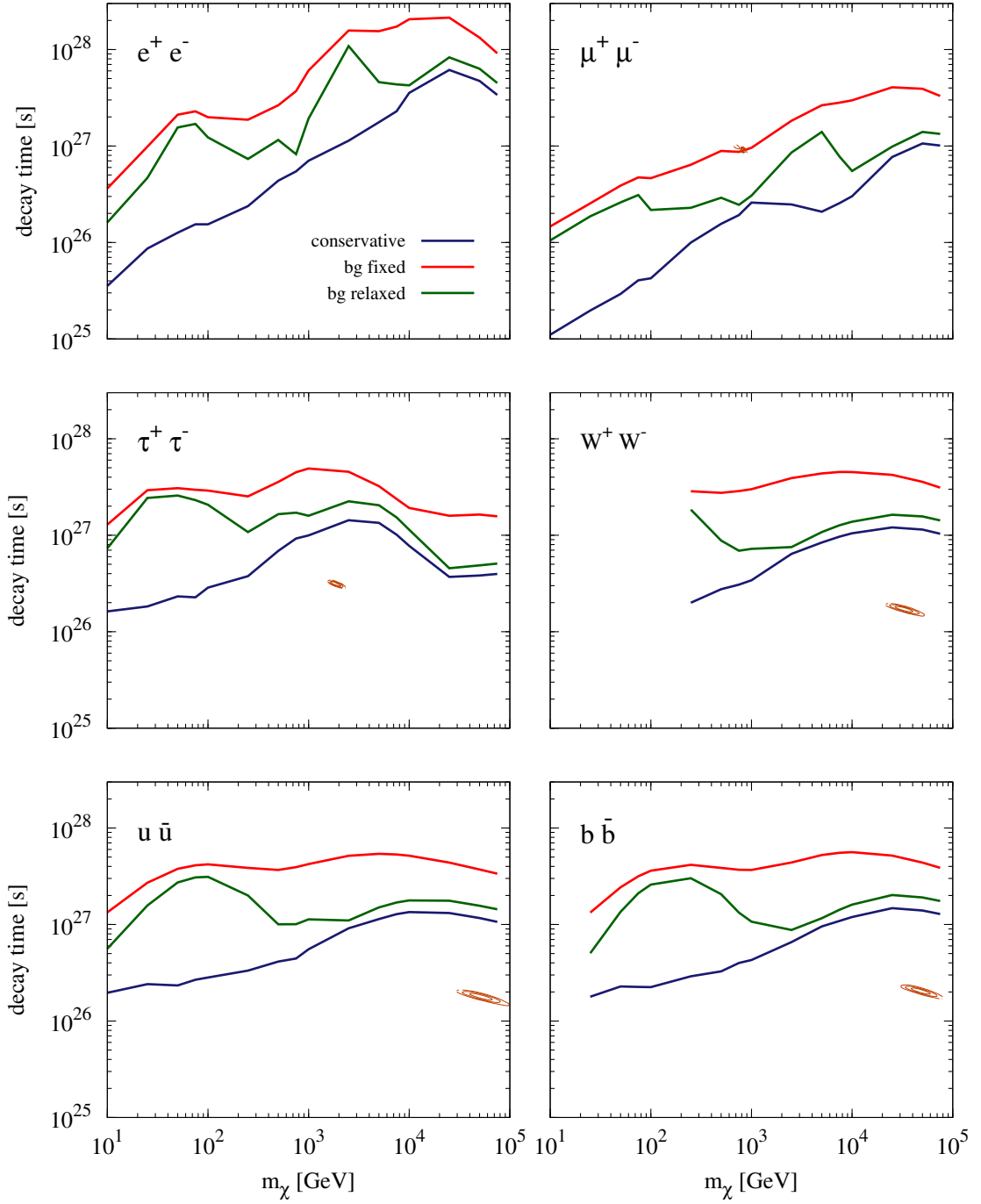


Fig. 6: The constraints of dark matter decay channels. Blue solid line is conservative limit, red solid line is the limit of background-fixed and green solid line is background-relaxed limits. The dark orange contours are the parameter space favored by the cosmic-ray electron-positron excess.

models, i.e. B01 [43] and M08 [44]. In our analysis, we derive three kinds of limits, namely conservative, background-fixed and background-relaxed limits. Compared with the conservative method, the background-fixed method can improve the constraints by about one order of magnitude at low DM masses. If a combined fit accounting for both DM-induced flux and the astrophysical background is performed, the corresponding background-relaxed limits always lie between the conservative and background-fixed limits.

For DM annihilation, we find the most stringent bounds are for $\tau^+\tau^-$ and $u\bar{u}$ channels. In the concentration parameter model is M08, the background-fixed limits for these two channels can be to the limits from the Fermi-LAT dwarf spheroidal galaxy observations in the mass region of $m_\chi \leq \mathcal{O}(10)$ GeV. For large DM masses $\sim \mathcal{O}(1)$ TeV, the constraints for the leptonic channels can be stronger than the dwarf galaxy limits. This indicates that the IGRB is suitable to search for heavy DM.

We also investigate the IGRB constraints on the parameter regions favored by the cosmic-ray electron-positron excess. We find that almost all the annihilation channels have been excluded by the background-fixed limits. Only the $\mu^+\mu^-$ channel remains valid by the conservative limit in the concentration model B01. For decaying DM, the most stringent constraint is set for the e^+e^- channel, which can reach even $\tau \sim 10^{28}$ s above several hundreds of GeV. Most decay channels favored by electron-positron anomaly have also been excluded by the conservative limits except the $\mu^+\mu^-$ channel. But the background-fixed limit is close to the border of its 3σ contours. The future observations will place more stringent constraint on this channel.

Acknowledgement

This work is supported by the National Natural Science Foundation of China under Grants No. 11475189, 11475191, 11135009, and by the 973 Program of China under Grant No. 2013CB837000, and by the Strategic Priority Research Program “The Emergence of Cosmological Structures” of the Chinese Academy of Sciences, under Grant No. XDB09000000. W. L. thanks Qiang Yuan, Bin Yue and Dahai Yan for helpful discussions of parameter constraint, structure formation and extragalactic background light.

Appendix A. Halo Mass Function

The halo mass function $dn(z)/dM_{\text{vir}}$ characterizes the comoving number density distribution of DM halos at different redshifts. It can be usually

written in the following widespread formula

$$\frac{dn(z)}{dM_{\text{vir}}} = \frac{\rho_{\chi}}{M_{\text{vir}}} \sqrt{\frac{2A^2a}{\pi}} [1 + (a\nu^2)^{-p}] \exp(-a\nu^2/2) \frac{d\nu}{dM_{\text{vir}}} \quad (\text{A.1})$$

with $(A, \alpha, p) = (0.322, 0.707, 0.3)$, i.e. the well-known Sheth-Tormen formula. $\nu = \delta_c(z)/\sigma(M_{\text{vir}})$ and $\delta_c(z) = 1.68[D(z=0)/D(z)]$ is the critical overdensity above which the spherical collapse occurs [63]. $D(z)$ is the linear growth factor representing the growth of the density perturbation inside the horizon after matter-radiation equality era. A prevailing approximation can be found in [64, 42],

$$D(z) \simeq \frac{5\Omega_m/2}{(1+z)[\Omega_m^{4/7} - \Omega_{\Lambda} + (1 + \Omega_m/2)(1 + \Omega_{\Lambda}/70)]}. \quad (\text{A.2})$$

$\sigma^2(M_{\text{vir}})$ is the average variance of the density field, which is evaluated by integrating the matter power spectrum in k-space

$$\sigma^2(M_{\text{vir}}) = \frac{1}{2\pi^2} \int W^2(kR_M) P_{\delta}(k) k^2 dk, \quad (\text{A.3})$$

where $W(x)$ is the window function. In the literature, two window functions are often met, i.e. the top-hat window function ($W(x) = 3(\sin x - x \cos x)/x^3$) and the Gaussian window function ($W(x) = \exp[-x^2/2]$). In this paper, we use the former one. $P_{\delta}(k)$ is the matter power spectrum given by

$$P_{\delta}(k) = A_s (k \cdot \text{Mpc})^{n_s} T^2(k). \quad (\text{A.4})$$

In above equation, constant A_s is normalized by $\sigma_8 \equiv \sigma(8h^{-1}\text{Mpc})$. $T(k)$ is the linear transfer function, and here we use its well-fitted form under adiabatic cold DM scenario with $\Omega_{b,0} \ll \Omega_{m,0}$ [65, 42]

$$T(q) = \frac{\ln(1 + 2.34q)}{2.34q} [1 + 3.89q + (16.1q)^2 + (5.46q)^3 + (6.71q)^4]^{-0.25}, \quad (\text{A.5})$$

where $q = k/\Gamma(h\text{Mpc}^{-1})$ and $\Gamma = \Omega_{m,0}h \exp[-\Omega_{b,0}(1 + \sqrt{2h}/\Omega_{m,0})]$ is to describe the horizon scale at t_{eq} .

Appendix B. Dark Matter Subhalos in the Galaxy

When the substructures bring forth, the DM densities with the same radius r are no longer the same. In [53], the authors defined a probability

density function $P(\rho, r)$, which represents at r the probability to take density between ρ and $\rho + d\rho$ is $P(\rho, r) d\rho$. If f_s denotes the fraction of smooth DM component, then $1 - f_s$ is that of the clumped component. According to the simulation, $f_s \sim 1$, so the clumpy component only occupies a tiny portion, i.e. $1 - f_s \ll 1$. The part of high DM density is postulated to have a power-law distribution. The probability distribution function $P(\rho, r)$ is

$$P(\rho; r) = \frac{f_s}{\sqrt{2\pi} \Delta^2} \frac{1}{\rho} \exp \left\{ -\frac{1}{2\Delta^2} \left[\ln \left(\frac{\rho}{\rho_h} e^{\Delta^2/2} \right) \right]^2 \right\} + (1 - f_s) \frac{1 + \alpha(r)}{\rho_h} \Theta(\rho - \rho_h) \left(\frac{\rho}{\rho_h} \right)^{-(2+\alpha)}. \quad (\text{B.1})$$

The first term comes from the smooth halo component, which has a log-normal distribution with the mean density ρ_h and variance Δ^2 . The second term is high-density power-law tail due to substructure. The fraction of smooth-halo part can be well-approximated by

$$f_s(r) = 1 - 7 \times 10^{-3} \left(\frac{\bar{\rho}(r)}{\bar{\rho}(r = 100 \text{ kpc})} \right)^{-0.26}, \quad (\text{B.2})$$

where $\bar{\rho}$ is given by the probabilistic average of ρ

$$\begin{aligned} \bar{\rho}(r) &= \int_0^{\rho_{\max}} \rho P(\rho) d\rho \\ &= f_s \rho_h + (1 - f_s) \rho_h \begin{cases} \frac{1+\alpha}{\alpha} \left[1 - \left(\frac{\rho_{\max}}{\rho_h} \right)^{-\alpha} \right]; & \alpha \neq 0, \\ \ln \frac{\rho_{\max}}{\rho_h}; & \alpha = 0, \end{cases} \end{aligned} \quad (\text{B.3})$$

where $\rho_{\max} = 80 \text{ GeV cm}^{-3}$. The enhancement due to substructures can be attributed to a boost factor $B(r)$, i.e.

$$\begin{aligned} B(r) &= \frac{\int \rho^2 dV}{\int [\bar{\rho}(r)]^2 dV} \\ &= \int_0^{\rho_{\max}} P(\rho, r) \frac{\rho^2}{[\bar{\rho}(r)]^2} d\rho, \\ &= f_s e^{\Delta^2} + (1 - f_s) \frac{1 + \alpha}{1 - \alpha} \left[\left(\frac{\rho_{\max}}{\rho_h} \right)^{1-\alpha} - 1 \right]. \end{aligned} \quad (\text{B.4})$$

The first term $f_s e^{\Delta^2}$ corresponds to the variation in the smooth component. Since from simulations $\Delta \lesssim 0.2$, it contributes to the overall boost factor by only a few percent and can be safely neglected.

References

- [1] Planck Collaboration, P. A. R. Ade, N. Aghanim, et al. Planck 2015 results. XIII. Cosmological parameters. ArXiv e-prints, February 2015.
- [2] M. Ackermann, M. Ajello, A. Albert, et al. The Spectrum of Isotropic Diffuse Gamma-Ray Emission between 100 MeV and 820 GeV. ApJ, 799:86, January 2015.
- [3] P. Sreekumar, D. L. Bertsch, B. L. Dingus, et al. EGRET Observations of the Extragalactic Gamma-Ray Emission. ApJ, 494:523–534, February 1998.
- [4] A. A. Abdo, M. Ackermann, M. Ajello, et al. Spectrum of the Isotropic Diffuse Gamma-Ray Emission Derived from First-Year Fermi Large Area Telescope Data. Physical Review Letters, 104(10):101101, March 2010.
- [5] M. Fornasa and M. A. Sánchez-Conde. The nature of the Diffuse Gamma-Ray Background. Phys. Rep., 598:1–58, October 2015.
- [6] P. Ullio, L. Bergström, J. Edsjö, and C. Lacey. Cosmological dark matter annihilations into γ rays: A closer look. Phys. Rev. D, 66(12):123502, December 2002.
- [7] J. E. Taylor and J. Silk. The clumpiness of cold dark matter: implications for the annihilation signal. MNRAS, 339:505–514, February 2003.
- [8] S. Profumo and T. E. Jeltema. Extragalactic Inverse Compton Light from Dark Matter annihilation and the Pamela positron excess. J. Cosmology Astropart. Phys., 7:20, July 2009.
- [9] M. Kawasaki, K. Kohri, and K. Nakayama. Diffuse gamma-ray background and cosmic-ray positrons from annihilating dark matter. Phys. Rev. D, 80(2):023517, July 2009.

- [10] A. A. Abdo, M. Ackermann, M. Ajello, et al. Constraints on cosmological dark matter annihilation from the Fermi-LAT isotropic diffuse gamma-ray measurement. J. Cosmology Astropart. Phys., 4:14, April 2010.
- [11] Q. Yuan, B. Yue, X.-J. Bi, X. Chen, and X. Zhang. Leptonic dark matter annihilation in the evolving universe: constraints and implications. J. Cosmology Astropart. Phys., 10:23, October 2010.
- [12] M. Cirelli, P. Panci, and P. D. Serpico. Diffuse gamma ray constraints on annihilating or decaying Dark Matter after Fermi. Nuclear Physics B, 840:284–303, November 2010.
- [13] C.-R. Chen, S. K. Mandal, and F. Takahashi. Gamma-ray constraints on hadronic and leptonic activities of decaying dark matter. J. Cosmology Astropart. Phys., 1:23, January 2010.
- [14] S. Blanchet and J. Lavalle. Diffuse gamma-ray constraints on dark matter revisited I: the impact of subhalos. J. Cosmology Astropart. Phys., 11:21, November 2012.
- [15] M. Cirelli, E. Moulin, P. Panci, P. D. Serpico, and A. Viana. Gamma ray constraints on decaying dark matter. Phys. Rev. D, 86(8):083506, October 2012.
- [16] K. N. Abazajian, S. Blanchet, and J. P. Harding. Current and future constraints on dark matter from prompt and inverse-Compton photon emission in the isotropic diffuse gamma-ray background. Phys. Rev. D, 85(4):043509, February 2012.
- [17] T. Bringmann, F. Calore, M. Di Mauro, and F. Donato. Constraining dark matter annihilation with the isotropic γ -ray background: Updated limits and future potential. Phys. Rev. D, 89(2):023012, January 2014.
- [18] I. Cholis, D. Hooper, and S. D. McDermott. Dissecting the gamma-ray background in search of dark matter. J. Cosmology Astropart. Phys., 2:14, February 2014.
- [19] The Fermi LAT Collaboration, M. Ackermann, M. Ajello, et al. Limits on Dark Matter Annihilation Signals from the Fermi LAT 4-year Measurement of the Isotropic Gamma-Ray Background. ArXiv e-prints, January 2015.

- [20] M. Ajello, D. Gasparri, M. Sánchez-Conde, et al. The Origin of the Extragalactic Gamma-Ray Background and Implications for Dark Matter Annihilation. ApJ, 800:L27, February 2015.
- [21] M. Di Mauro and F. Donato. The composition of the Fermi-LAT IGRB intensity: emission from extragalactic point sources and dark matter annihilations. ArXiv e-prints, January 2015.
- [22] S. Ando and K. Ishiwata. Constraints on decaying dark matter from the extragalactic gamma-ray background. ArXiv e-prints, February 2015.
- [23] J.-Q. Xia, A. Cuoco, E. Branchini, and M. Viel. Tomography of the Fermi-LAT γ -Ray Diffuse Extragalactic Signal via Cross Correlations with Galaxy Catalogs. ApJS, 217:15, March 2015.
- [24] A. Cuoco, J.-Q. Xia, M. Regis, et al. Dark matter searches in the gamma-ray extragalactic background via cross-correlations with galaxy catalogues. ArXiv e-prints, June 2015.
- [25] O. Adriani, G. C. Barbarino, G. A. Bazilevskaya, et al. An anomalous positron abundance in cosmic rays with energies 1.5-100GeV. Nature, 458:607–609, April 2009.
- [26] J. Chang, J. H. Adams, H. S. Ahn, et al. An excess of cosmic ray electrons at energies of 300-800GeV. Nature, 456:362–365, November 2008.
- [27] A. A. Abdo, M. Ackermann, M. Ajello, et al. Measurement of the Cosmic Ray $e^+ + e^-$ Spectrum from 20GeV to 1TeV with the Fermi Large Area Telescope. Physical Review Letters, 102(18):181101, May 2009.
- [28] L. Accardo, M. Aguilar, D. Aisa, et al. High Statistics Measurement of the Positron Fraction in Primary Cosmic Rays of 0.5-500 GeV with the Alpha Magnetic Spectrometer on the International Space Station. Physical Review Letters, 113(12):121101, September 2014.
- [29] M. Aguilar, D. Aisa, A. Alvino, et al. Electron and Positron Fluxes in Primary Cosmic Rays Measured with the Alpha Magnetic Spectrometer on the International Space Station. Physical Review Letters, 113(12):121102, September 2014.

- [30] I. V. Moskalenko and A. W. Strong. Production and Propagation of Cosmic-Ray Positrons and Electrons. ApJ, 493:694–707, January 1998.
- [31] A. W. Strong and I. V. Moskalenko. Propagation of Cosmic-Ray Nucleons in the Galaxy. ApJ, 509:212–228, December 1998.
- [32] C. Consolandi and on Behalf of the AMS-02 Collaboration. Primary Cosmic Ray Proton Flux Measured by AMS-02. ArXiv e-prints, February 2014.
- [33] Ams-02 collaboration. <http://www.ams02.org>, 2013.
- [34] S.-J. Lin, Q. Yuan, and X.-J. Bi. Quantitative study of the AMS-02 electron/positron spectra: Implications for pulsars and dark matter properties. Phys. Rev. D, 91(6):063508, March 2015.
- [35] S.-J. Lin, X.-J. Bi, P.-F. Yin, and Z.-H. Yu. Implications for dark matter annihilation from the AMS-02 \bar{p}/p ratio. ArXiv e-prints, April 2015.
- [36] K. A. Olive and Particle Data Group. Review of Particle Physics. Chinese Physics C, 38(9):090001, August 2014.
- [37] M. Cirelli, G. Corcella, A. Hektor, et al. PPC 4 DM ID: a poor particle physicist cookbook for dark matter indirect detection. J. Cosmology Astropart. Phys., 3:51, March 2011.
- [38] F. C. Jones. Calculated Spectrum of Inverse-Compton-Scattered Photons. Physical Review, 167:1159–1169, March 1968.
- [39] G. R. Blumenthal and R. J. Gould. Bremsstrahlung, Synchrotron Radiation, and Compton Scattering of High-Energy Electrons Traversing Dilute Gases. Reviews of Modern Physics, 42:237–271, 1970.
- [40] J. F. Navarro, C. S. Frenk, and S. D. M. White. The Structure of Cold Dark Matter Halos. ApJ, 462:563, May 1996.
- [41] G. L. Bryan and M. L. Norman. Statistical Properties of X-Ray Clusters: Analytic and Numerical Comparisons. ApJ, 495:80–99, March 1998.

- [42] H. Mo, F. C. van den Bosch, and S. White. Galaxy Formation and Evolution. Cambridge University Press, 2010, May 2010.
- [43] J. S. Bullock, T. S. Kolatt, Y. Sigad, et al. Profiles of dark haloes: evolution, scatter and environment. MNRAS, 321:559–575, March 2001.
- [44] A. V. Macciò, A. A. Dutton, and F. C. van den Bosch. Concentration, spin and shape of dark matter haloes as a function of the cosmological model: WMAP1, WMAP3 and WMAP5 results. MNRAS, 391:1940–1954, December 2008.
- [45] Q. Yuan, P.-F. Yin, X.-J. Bi, X.-M. Zhang, and S.-H. Zhu. Gamma rays and neutrinos from dark matter annihilation in galaxy clusters. Phys. Rev. D, 82(2):023506, July 2010.
- [46] R. C. Gilmore, R. S. Somerville, J. R. Primack, and A. Domínguez. Semi-analytic modelling of the extragalactic background light and consequences for extragalactic gamma-ray spectra. MNRAS, 422:3189–3207, June 2012.
- [47] L. J. Rosenberg and K. A. van Bibber. Searches for invisible axions. Phys. Rep., 325:1–39, February 2000.
- [48] S. J. Asztalos, L. J. Rosenberg, K. van Bibber, P. Sikivie, and K. Zioutas. Searches for Astrophysical and Cosmological Axions. Annual Review of Nuclear and Particle Science, 56:293–326, November 2006.
- [49] J. F. Navarro, C. S. Frenk, and S. D. M. White. A Universal Density Profile from Hierarchical Clustering. ApJ, 490:493–508, December 1997.
- [50] C. Giocoli, G. Tormen, R. K. Sheth, and F. C. van den Bosch. The substructure hierarchy in dark matter haloes. MNRAS, 404:502–517, May 2010.
- [51] M. Maciejewski, M. Vogelsberger, S. D. M. White, and V. Springel. Bound and unbound substructures in Galaxy-scale dark matter haloes. MNRAS, 415:2475–2484, August 2011.
- [52] M. Kamionkowski and S. M. Koushiappas. Galactic substructure and direct detection of dark matter. Phys. Rev. D, 77(10):103509, May 2008.

- [53] M. Kamionkowski, S. M. Koushiappas, and M. Kuhlen. Galactic substructure and dark-matter annihilation in the Milky Way halo. Phys. Rev. D, 81(4):043532, February 2010.
- [54] T. M. Venters and V. Pavlidou. The Effect of Blazar Spectral Breaks on the Blazar Contribution to the Extragalactic Gamma-Ray Background. ApJ, 737:80, August 2011.
- [55] H. D. Zeng, D. H. Yan, Y. Q. Sun, and L. Zhang. γ -Ray Luminosity Function and the Contribution to Extragalactic γ -Ray Background for Fermi-detected Blazars. ApJ, 749:151, April 2012.
- [56] H. Zeng, D. Yan, and L. Zhang. A revisit of gamma-ray luminosity function and contribution to the extragalactic diffuse gamma-ray background for Fermi FSRQs. MNRAS, 431:997–1003, May 2013.
- [57] M. Ackermann, M. Ajello, A. Allafort, et al. GeV Observations of Star-forming Galaxies with the Fermi Large Area Telescope. ApJ, 755:164, August 2012.
- [58] B. C. Lacki, S. Horiuchi, and J. F. Beacom. The Star-forming Galaxy Contribution to the Cosmic MeV and GeV Gamma-Ray Background. ApJ, 786:40, May 2014.
- [59] Y. Inoue. Contribution of Gamma-Ray-loud Radio Galaxies’ Core Emissions to the Cosmic MeV and GeV Gamma-Ray Background Radiation. ApJ, 733:66, May 2011.
- [60] M. Di Mauro, F. Calore, F. Donato, M. Ajello, and L. Latronico. Diffuse γ -Ray Emission from Misaligned Active Galactic Nuclei. ApJ, 780:161, January 2014.
- [61] The Fermi-LAT Collaboration. Resolving the Extragalactic γ -ray Background above 50 GeV with Fermi-LAT. ArXiv e-prints, November 2015.
- [62] M. Ackermann, A. Albert, B. Anderson, et al. Dark matter constraints from observations of 25 Milky Way satellite galaxies with the Fermi Large Area Telescope. Phys. Rev. D, 89(4):042001, February 2014.
- [63] V. R. Eke, S. Cole, and C. S. Frenk. Cluster evolution as a diagnostic for Omega. MNRAS, 282:263–280, September 1996.

- [64] S. M. Carroll, W. H. Press, and E. L. Turner. The cosmological constant. ARA&A, 30:499–542, 1992.
- [65] J. M. Bardeen, J. R. Bond, N. Kaiser, and A. S. Szalay. The statistics of peaks of Gaussian random fields. ApJ, 304:15–61, May 1986.